Electronic Supplementary Material (ESI) for Inorganic Chemistry Frontiers.

Supporting Information

Importance of the Iron Valence State in NiCoFe Nanosheet Array Catalysts for the Oxygen Evolution Reaction

Hua-Shuai Hu, Yang Li, Gao Deng, Ya-Ru Shao, Ke-Xin Li, Chong-Bin Wang, Yuan-Yuan Feng*

Key laboratory of Life-organic Analysis, College of Chemistry and Chemical Engineering, Qufu Normal University, Qufu Shandong, 273165, China

* E-mail: yfeng@mail.tsinghua.edu.cn

Contents

The Krasil'shcikov path:

Generally, the commonly accepted mechanism of OER in alkaline media abides by the Krasil'shcikov path, as shown in the following equations (S1-S4).[1]

$$* + OH^- \rightarrow *\text{-}OH + e^- \quad \text{(S1)}$$

$$*\text{-}OH + OH^- \rightarrow *\text{-}O^- + H_2O \quad \text{(S2)}$$

$$*\text{-}O^- \rightarrow *\text{-}O + e^- \quad \text{(S3)}$$

$$2*\text{-}O \rightarrow 2* + O_2\uparrow \quad \text{(S4)}$$

* represents an active site.

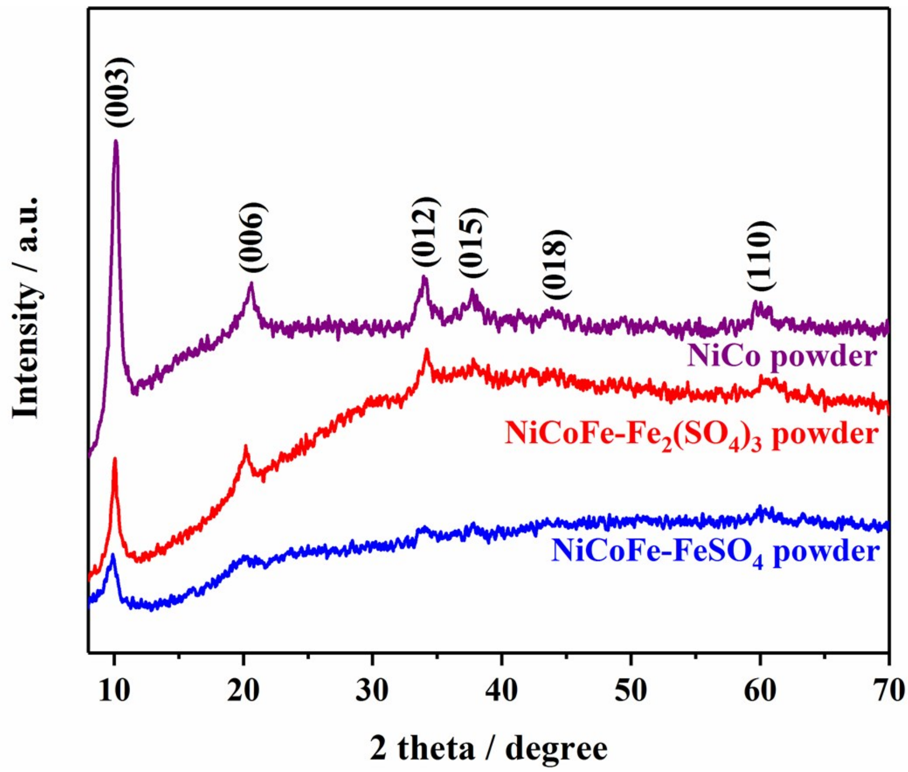

Figure S1. XRD patterns of NiCo powder, NiCoFe-$Fe_2(SO_4)_3$ powder and NiCoFe-$FeSO_4$ powder samples.

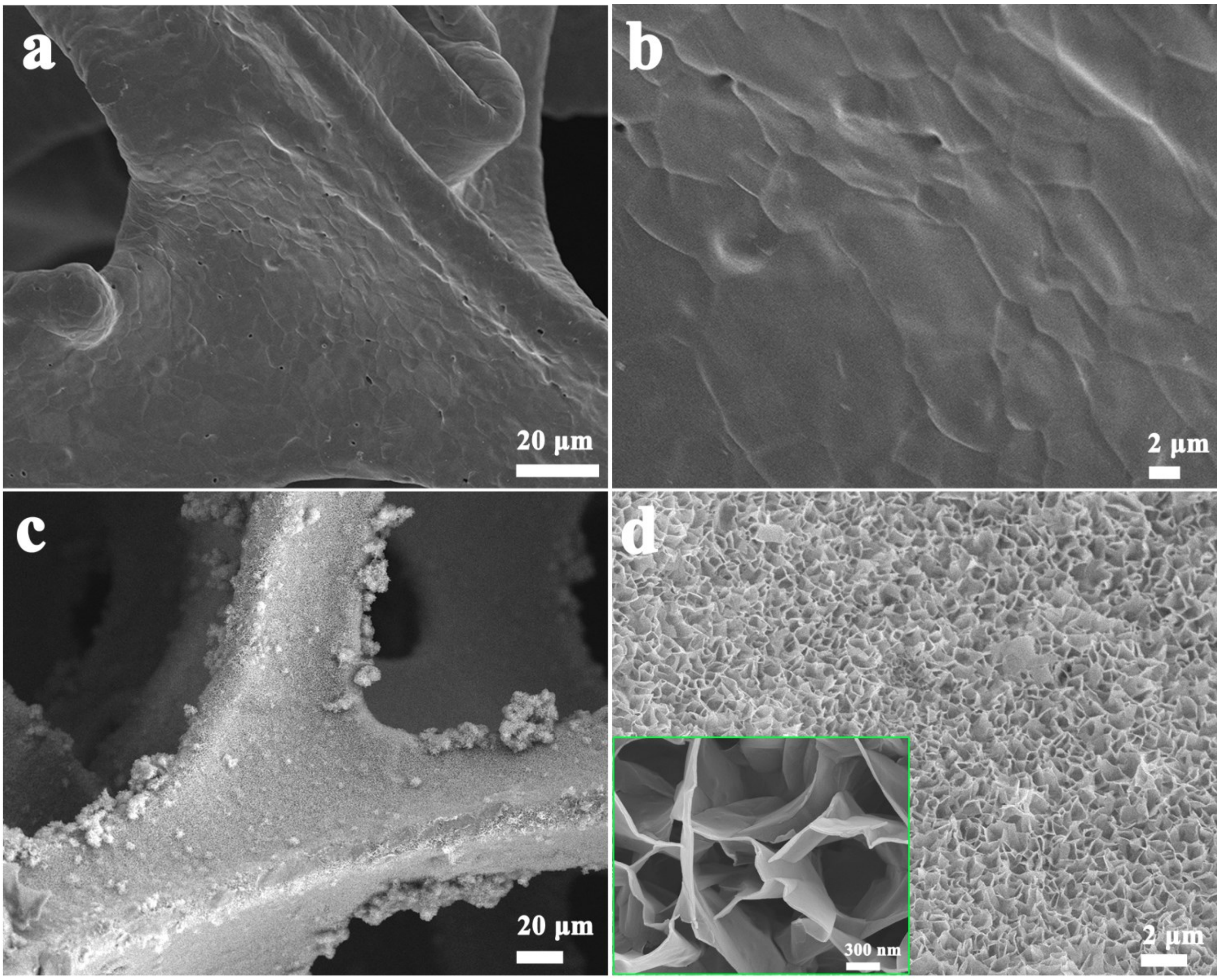

Figure S2. SEM images of (a, b) bare NF and (c, d) NiCo/NF. Inset of (d) shows the enlarged SEM image.

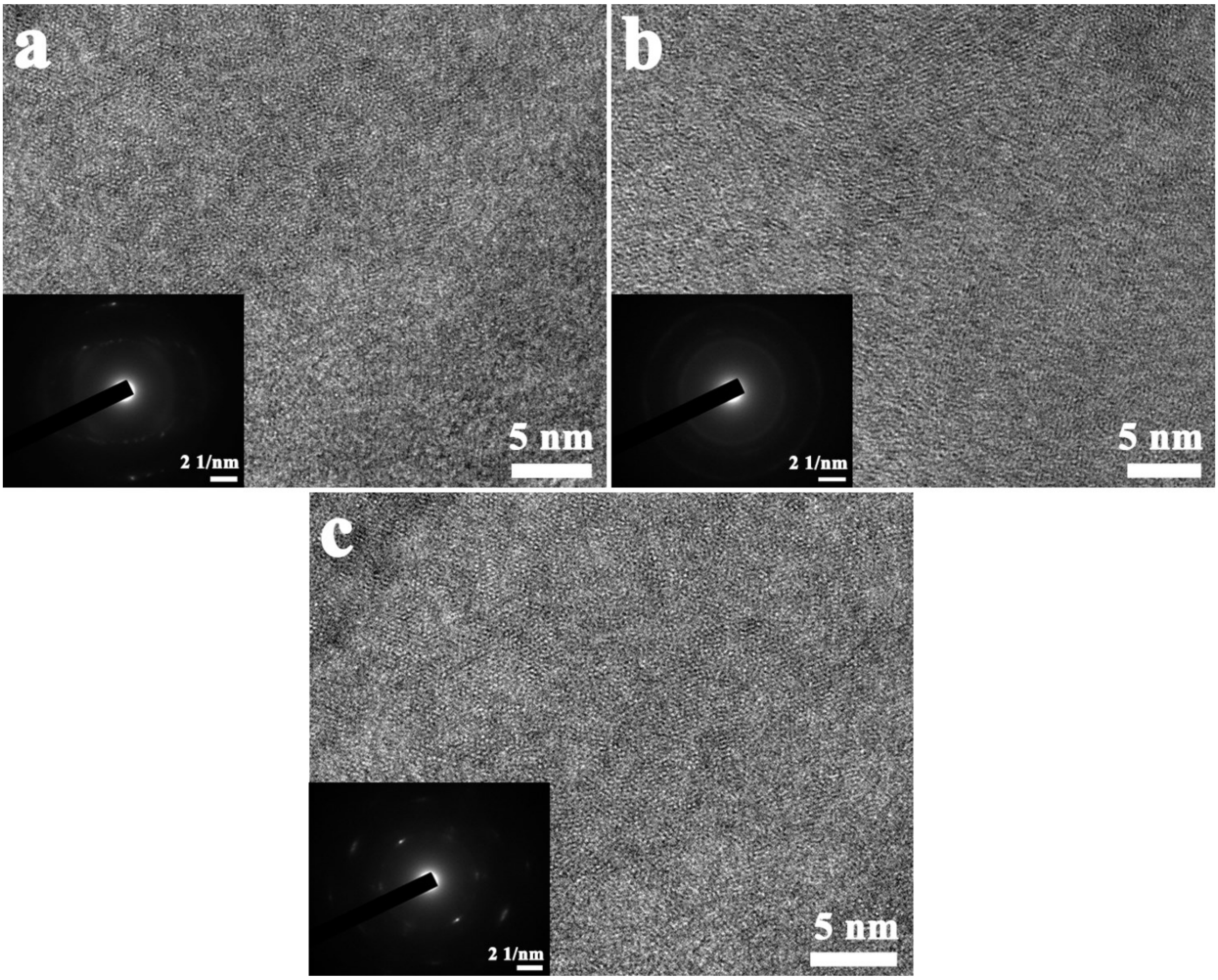

Figure S3. (a-c) The HRTEM and selected area electron diffraction patterns measured from different regions of the NiCoFe/NF-$FeSO_4$ sample.

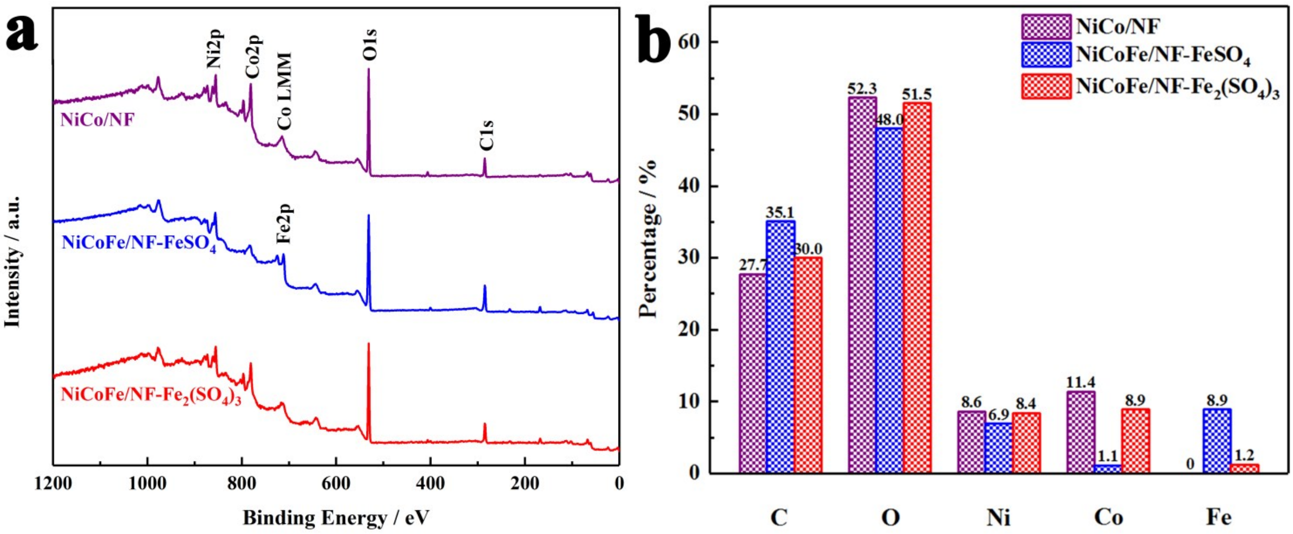

Figure S4. (a) XPS surveys of NiCo/NF, NiCoFe/NF-$FeSO_4$ and NiCoFe/NF-$Fe_2(SO_4)_3$. (b) The chemical compositions of NiCo/NF, NiCoFe/NF-$FeSO_4$ and NiCoFe/NF-$Fe_2(SO_4)_3$ obtained from the XPS results.

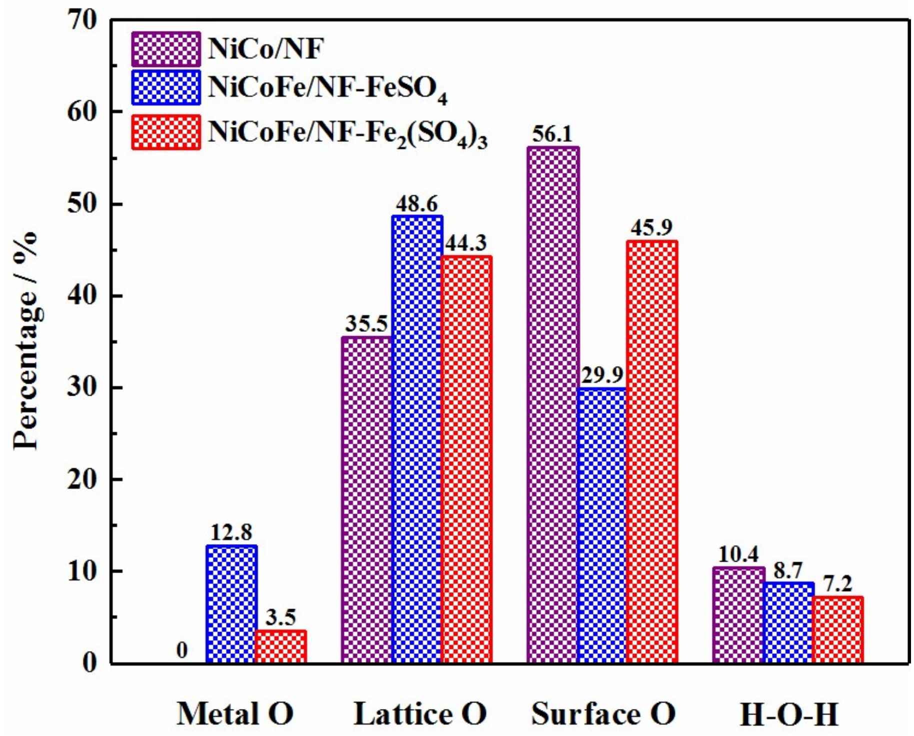

Figure S5. The percentage of various chemical states of O in NiCo/NF, NiCoFe/NF-$FeSO_4$ and NiCoFe/NF-$Fe_2(SO_4)_3$ obtained by XPS.

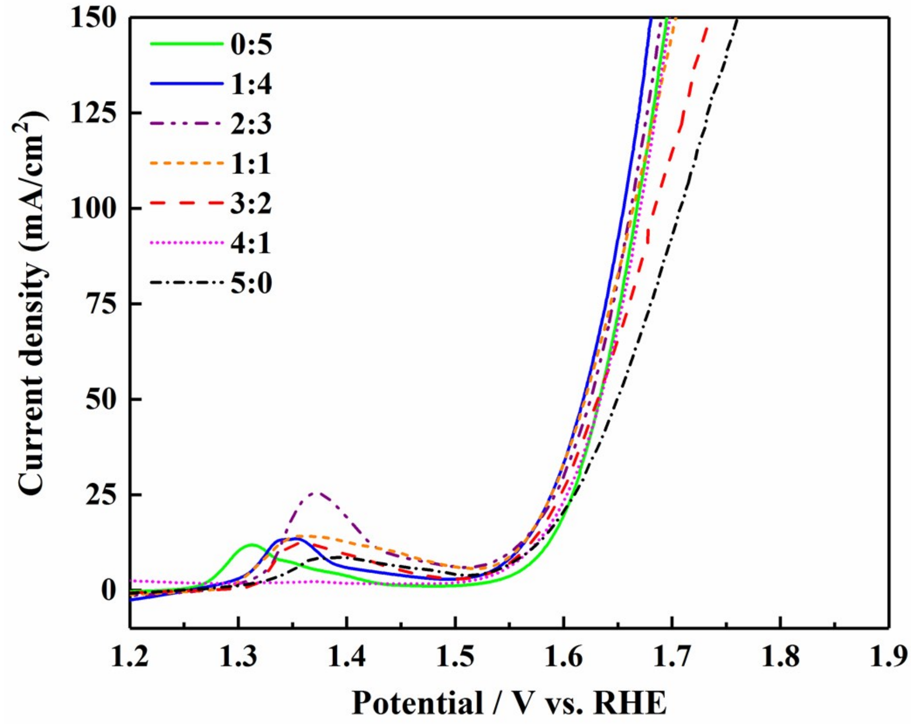

Figure S6. Linear sweep voltammetry curves of the NiCo/NF catalysts with different mole ratios of Ni/Co.

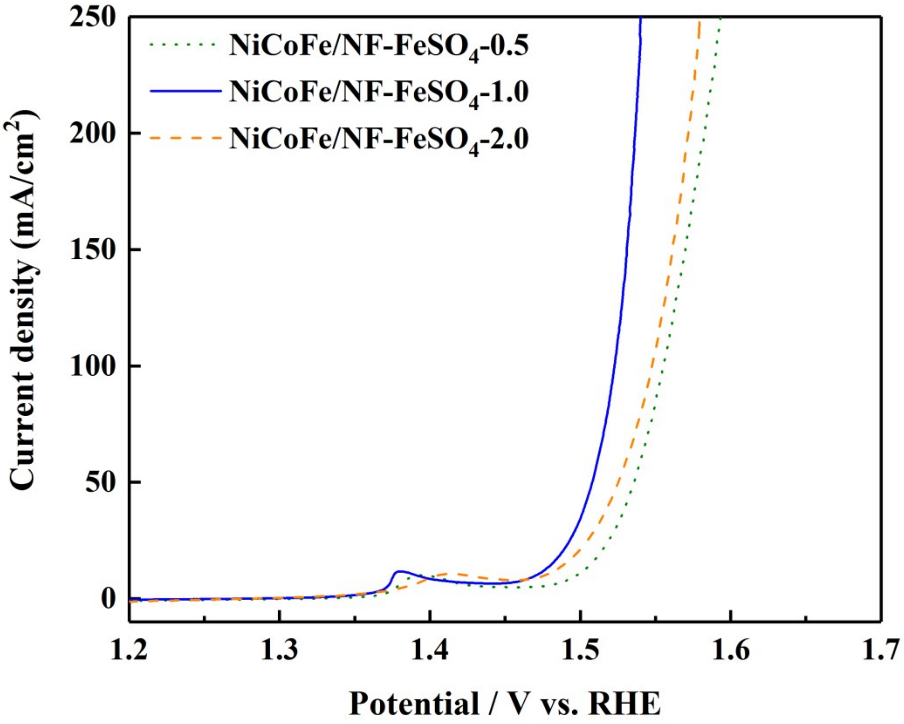

Figure S7. Linear sweep voltammetry curves of NiCoFe/NF-$FeSO_4$ catalysts prepared for different immersion time during cation exchange reaction.

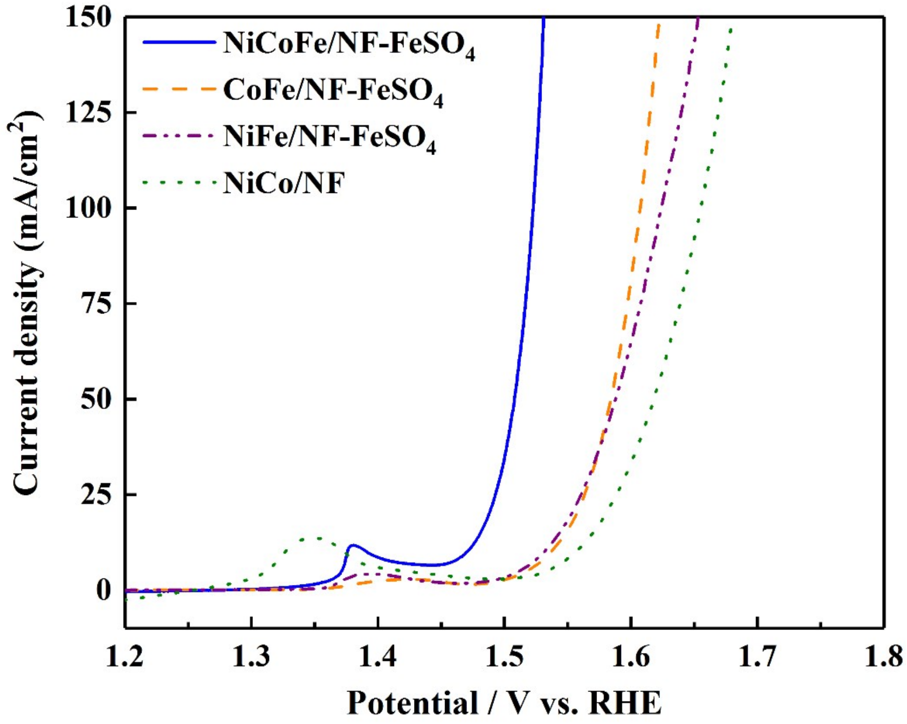

Figure S8. Linear sweep voltammetry curves of NiCoFe/NF-$FeSO_4$, CoFe/NF-$FeSO_4$, NiFe/NF-$FeSO_4$ and NiCo/NF.

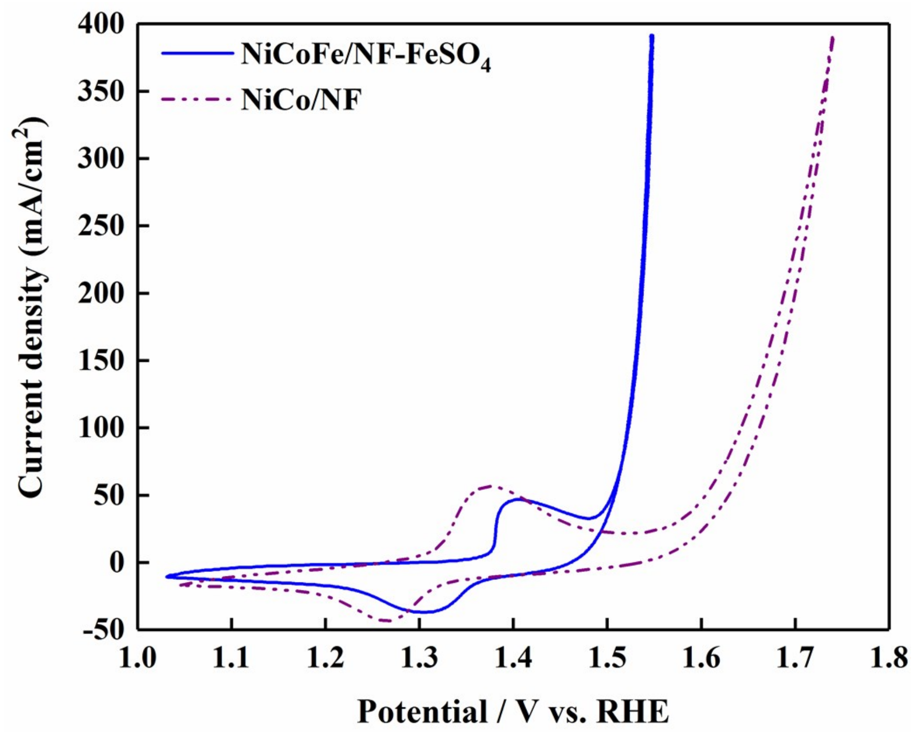

Figure S9. Cyclic voltammetry curves of NiCoFe/NF-$FeSO_4$ and NiCo/NF in 1.0 M KOH.

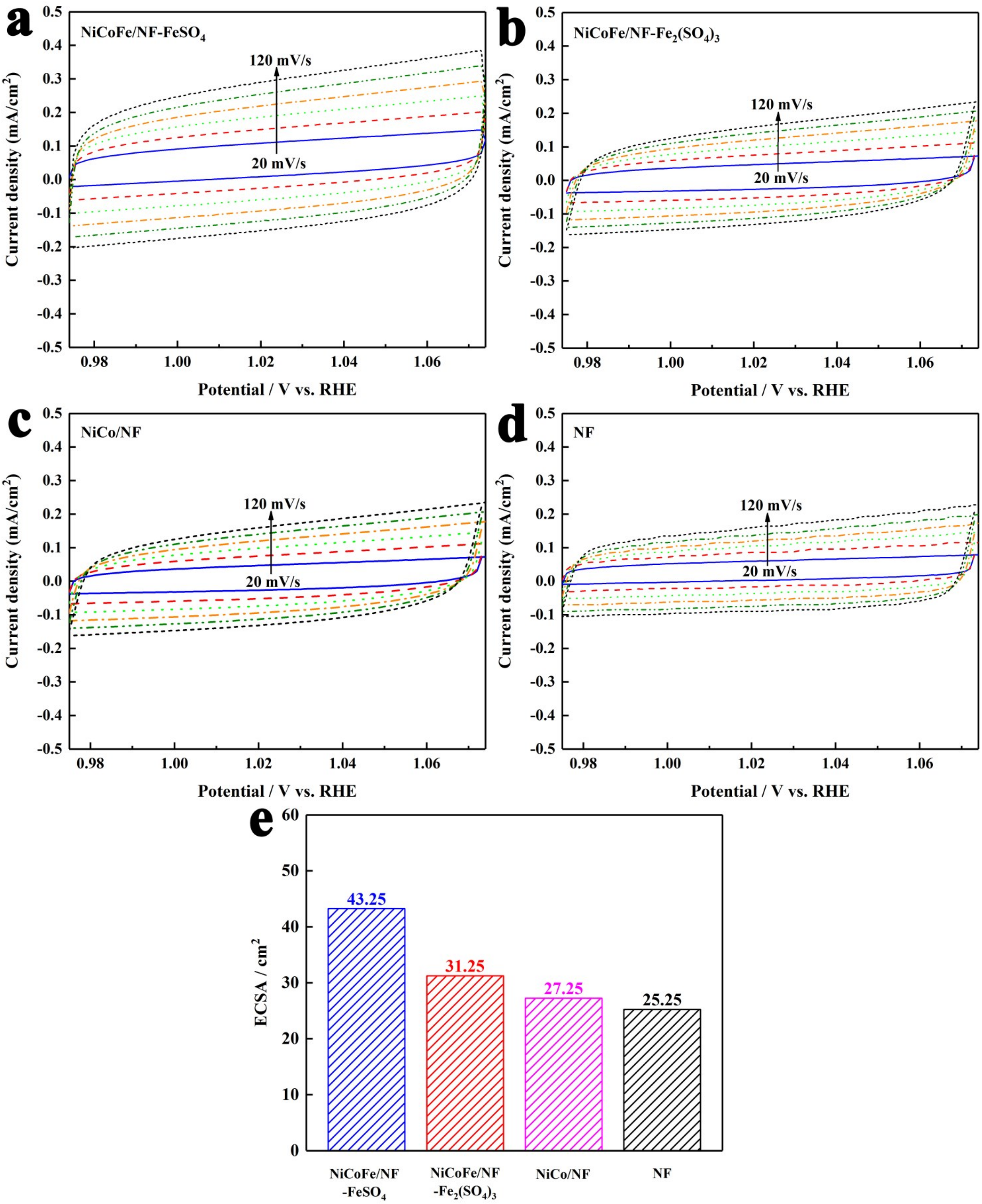

Figure S10. Cyclic voltammetry curves at different scanning rates (a-d), electrochemical surface area (e) of the NiCoFe/NF-FeSO$_4$, NiCoFe/NF-Fe$_2$(SO$_4$)$_3$, NiCo/NF and bare NF.

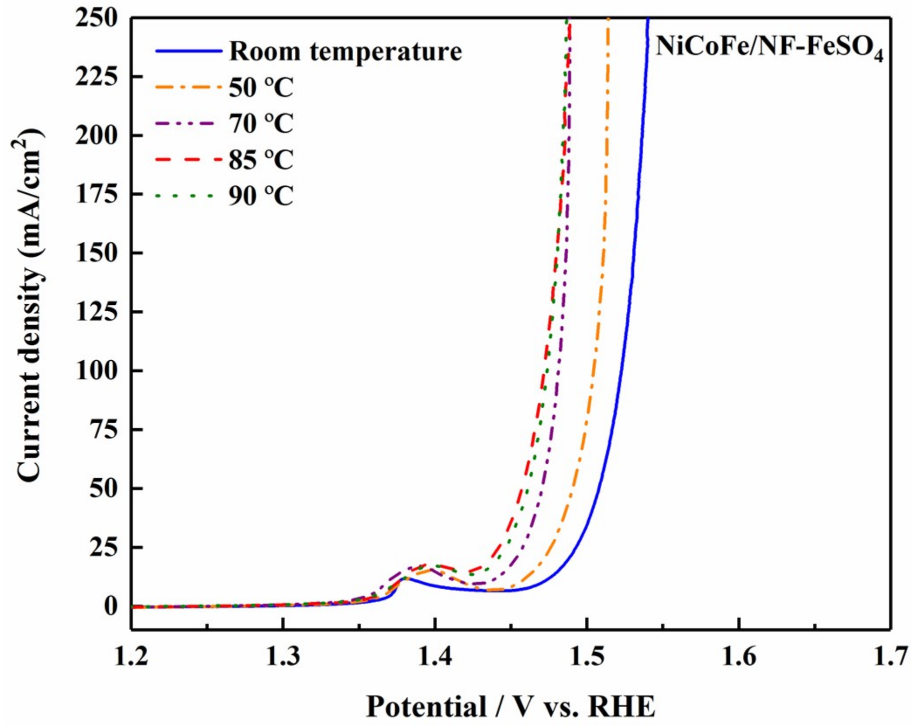

Figure S11. Linear sweep voltammetry curves of NiCoFe/NF-$FeSO_4$ at different temperatures.

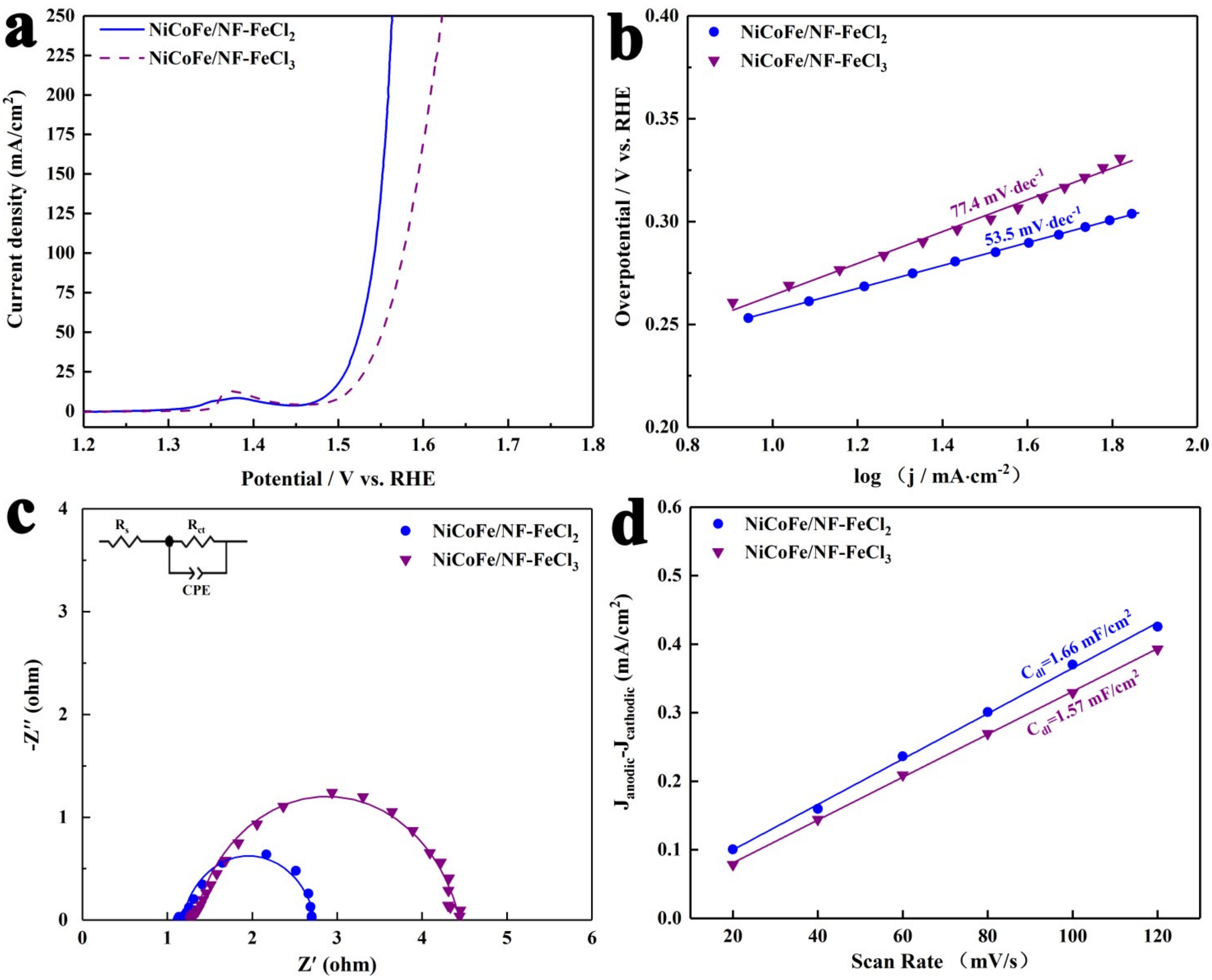

Figure S12. (a) Linear sweep voltammetry curves, (b) Tafel plots, (c) electrochemical impedance spectra and (d) double-layer capacitance of NiCoFe/NF-$FeCl_2$ and NiCoFe/NF-$FeCl_3$.

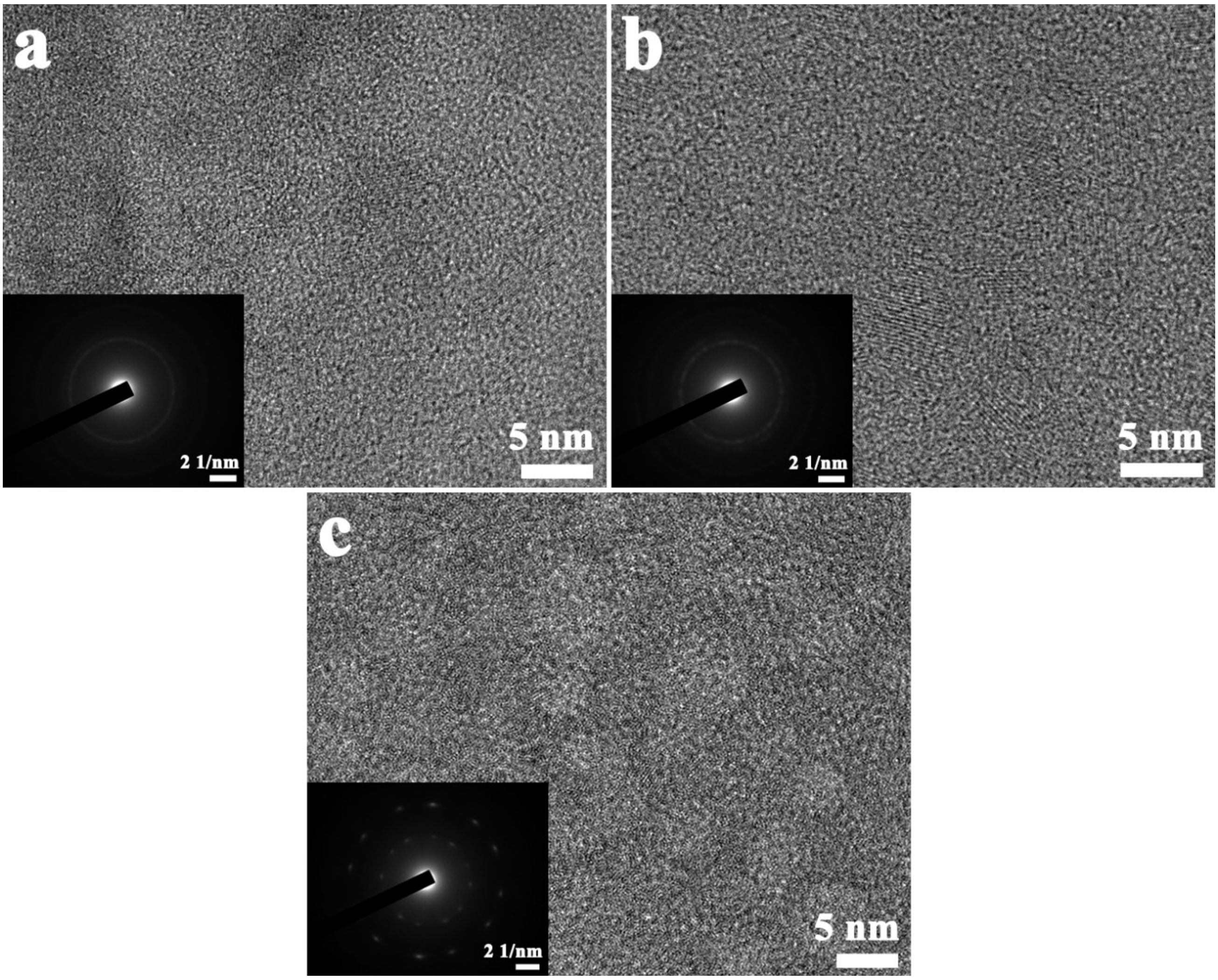

Figure S13. (a-c) The HRTEM and selected area electron diffraction patterns measured from different regions of the NiCoFe/NF-$FeSO_4$ sample after durability test in 1.0 M KOH.

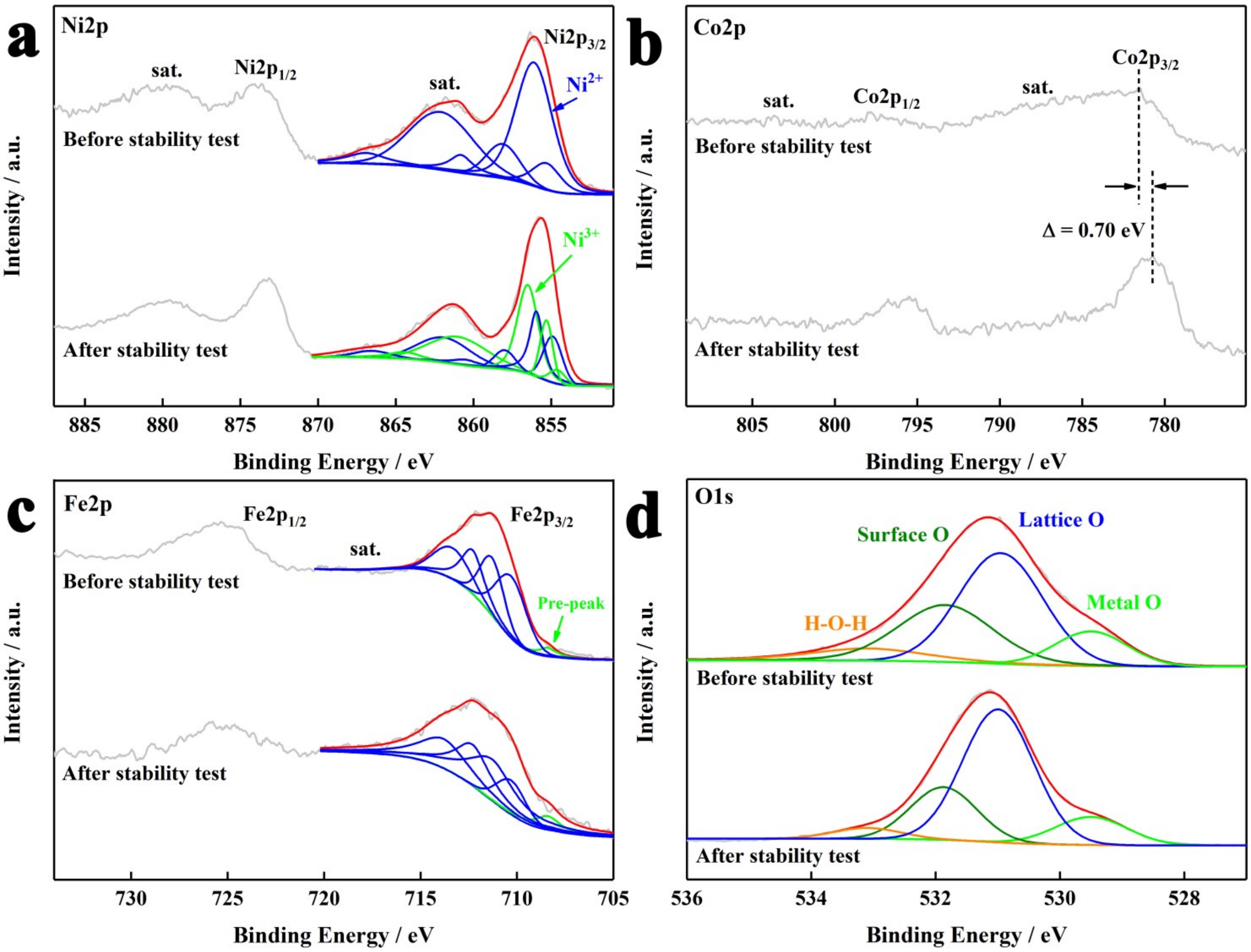

Figure S14. XPS spectra of Ni2p (a), Co2p (b), Fe2p (c) and O1s (d) of the NiCoFe/NF-$FeSO_4$ catalyst after 95 h of durability test in 1.0 M KOH.

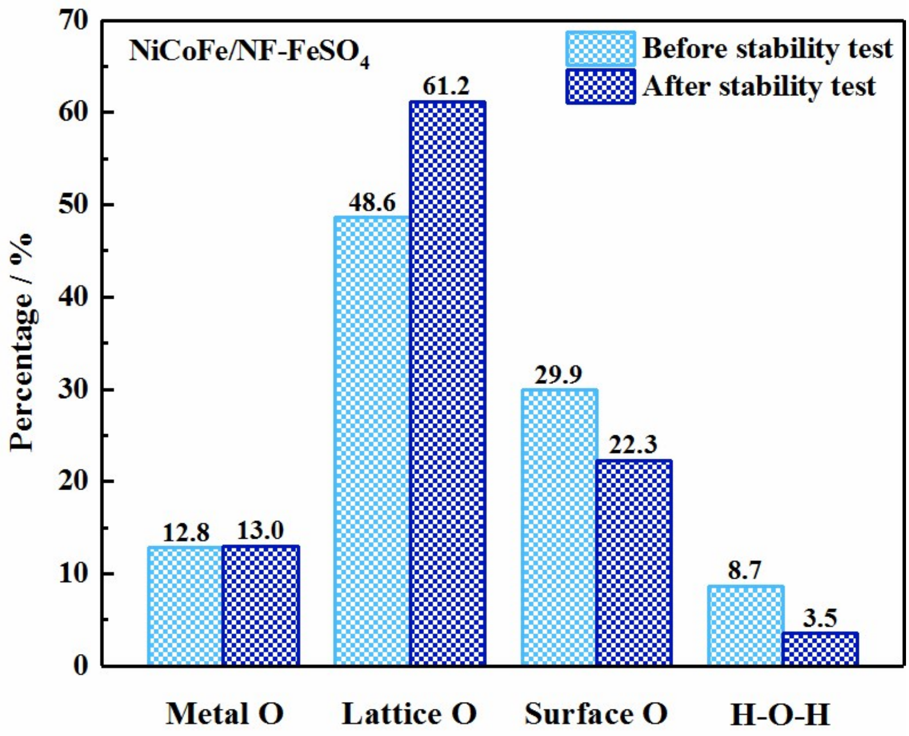

Figure S15. The percentage of different O species in NiCoFe/NF-$FeSO_4$ before and after the stability test based on the XPS results.

Table S1. The binding energy (eV) of $Ni2p_{3/2}$ spectra of different catalysts

Catalysts	Ni (II)					
	Peak 1	Peak 2	Peak 3	Peak 4	Peak 5	Peak 6
NiCo/NF	854.9	855.7	857.7	860.5	861.8	866.7
NiCoFe/NF-$FeSO_4$	855.1	856.1	858.1	860.8	862.1	866.9
NiCoFe/NF-$Fe_2(SO_4)_3$	854.9	855.7	857.7	860.5	861.8	866.7

Table S2. The binding energy (eV) of $Co2p_{3/2}$ spectra of different catalysts

Catalysts	Co(III)				Co(II)			
	Peak 1	Peak 2	Peak 3	Peak 4	Peak 5	Peak 6	Peak 7	Peak 8
NiCo/NF	780.1	781.4	783.1	790.2	780.4	782.2	786.0	789.2
NiCoFe/NF-$Fe_2(SO_4)_3$	780.1	781.4	783.1	790.2	780.4	782.2	786.0	789.2

Table S3. The binding energy (eV) of $Fe2p_{3/2}$ spectra of NiCoFe/NF-$FeSO_4$

Catalysts	Pre-peak	Fe(III)			
	Peak 1	Peak 2	Peak 3	Peak 4	Peak 5
NiCoFe/NF-$FeSO_4$	708.4	710.3	711.3	712.3	713.4

Table S4. The binding energy (eV) of O1s spectra of different catalysts

Catalysts	Metal O	Lattice O	Surface O	H-O-H
NiCo/NF	-	530.8	531.8	533.1
NiCoFe/NF-$FeSO_4$	529.5	530.8	531.8	533.1
NiCoFe/NF-$Fe_2(SO_4)_3$	529.5	530.8	531.8	533.1

Table S5. The binding energy (eV) of $Ni2p_{3/2}$ spectra of NiCoFe/NF-$FeSO_4$ after the stability test

Catalysts	Ni(III)				
	Peak 1	Peak 2	Peak 3	Peak 4	Peak 5
NiCoFe/NF-$FeSO_4$ (After stability test)	854.6	855.3	856.5	861.0	864.4

Table S6. Catalytic properties for OER of the Fe, Ni and Co-based electrocatalysts in alkaline electrolyte

Catalysts	Electrolyte	Current density (*j*)	Overpotentialat the Corresponding *j*	Stability test	Reference
NiCoFe/NF-FeSO$_4$	**1 M KOH**	**100 mA/cm^2** **300 mA/cm^2**	**293 mV** **313 mV**	**95 h** **-**	**This work**
NM50-Ni$_3$S$_4$/NF	1 M KOH	50 mA/cm^2 100 mA/cm^2	300 mV 340 mV	300 h -	2
hcp-NiFe@NC	1 M KOH	10 mA/cm^2 20 mA/cm^2 100 mA/cm^2	226 mV - 263 mV	- 35 h -	3
NiV-LDH@FeOOH/NF	1 M KOH	100 mA/cm^2	297 mV	20 h	4
pa-NiFe LDH NS/NIF	1 M KOH	100 mA/cm^2 140 mA/cm^2	326 mV 370 mV	- 5 h	5
FeMOF/NiMOF/NF	1 M KOH	100 mA/cm^2	359 mV	24 h	6
FeNiO$_x$H$_y$/NF	1 M KOH	10 mA/cm^2 100 mA/cm^2 1000 mA/cm^2	195 mV 241 mV 306 mV	- 20 h 80 h	7
CuS$_{0.55}$ HNP/CF	1 M KOH	100 mA/cm^2	386 mV	20 h	8
NiFe$_2$O$_4$/NiFe LDH/NF	1 M KOH	80 mA/cm^2 100 mA/cm^2 500 mA/cm^2	202 mV 213 mV 242 mV	20 h - 20 h	9
CoSn$_2$/NF	1 M KOH	10 mA/cm^2 100 mA/cm^2	230 mV 352 mV	16 h -	10
Ni$_2$Fe$_8$/NF	1 M KOH	10 mA/cm^2 100 mA/cm^2	186 mV 280 mV	42 h -	11
NiFe/NF	1 M KOH	10 mA/cm^2 100 mA/cm^2	215 mV -	- 10 h	12
Fe11%-NiO/NF	1 M KOH	10 mA/cm^2 20 mA/cm^2 100 mA/cm^2	206 mV - 268 mV	- 20 h -	13
NiCoFeP/NF	1 M KOH	100 mA/cm^2 200 mA/cm^2	- 271 mV	10 h -	14
NiS/NF	1 M KOH	20 mA/cm^2 50 mA/cm^2	290 mV 335 mV	20 h -	15
S:CoP@NF	1 M KOH	10 mA/cm^2 80 mA/cm^2 100 mA/cm^2	270 mV 350 mV 360 mV	- 20 h -	16
CoMoO$_4$-Ni(OH)$_2$/NF-400s	1 M KOH	50 mA/cm^2 100 mA/cm^2	320 mV 349 mV	100 h -	17

REFERENCES

1 S. Gupta, L. Qiao, S. Zhao, H. Xu, Y. Lin, S. V. Devaguptapu, X. Wang, M. T. Swihart and G. Wu, Highly Active and Stable Graphene Tubes Decorated with FeCoNi Alloy Nanoparticles via a Template-Free Graphitization for Bifunctional Oxygen Reduction and Evolution, *Adv. Energy Mater.*, 2016, **6**, 1601198.

2 K. Wan, J. Luo, C. Zhou, T. Zhang, J. Arbiol, X. Lu, B. Mao, X. Zhang and J. Fransaer, Hierarchical Porous Ni_3S_4 with Enriched High-Valence Ni Sites as a Robust Electrocatalyst for Efficient Oxygen Evolution Reaction, *Adv. Funct. Mater.*, 2019, **29**, 1900315.

3 C. Wang, H. Yang, Y. Zhang and Q. Wang, NiFe Alloy Nanoparticle with hcp Crystal Structure Stimulates Superior Oxygen Evolution Reaction Electrocatalytic Activity, *Angew. Chem., Int. Ed.*, 2019, **58**, 6099-6103.

4 W. Bao, L. Xiao, J. Zhang, Z. Deng, C. Yang, T. Ai and X. Wei, Interface engineering of NiV-LDH@FeOOH heterostructures as high-performance electrocatalysts for oxygen evolution reaction in alkaline conditions, *Chem. Commun.*, 2020, **56**, 9360-9363.

5 J. Xie, H. Qu, F. Lei, X. Peng, W. Liu, L. Gao, P. Hao, G. Cui and B. Tang, Partially amorphous nickel-iron layered double hydroxide nanosheet arrays for robust bifunctional electrocatalysis, *J. Mater. Chem. A*, 2018, **6**, 16121-16129.

6 D. Xiong, M. Gu, C. Chen, C. Lu, F. Y. Yi and X. Ma, Rational design of bimetallic metal-organic framework composites and their derived sulfides with superior electrochemical performance to remarkably boost oxygen evolution and supercapacitors, *Chem. Eng. J.*, 2021, **404**, 127111.

7 H. S. Hu, S. Si, R. J. Liu, C. B. Wang and Y. Y. Feng, Iron-nickel hydroxide nanoflake arrays supported on nickel foam with dramatic catalytic properties for the evolution of oxygen at high current densities, *Int. J. Energy Res.*, 2020, **44**, 9222-9232.

8 H. Zhang, H. Jiang, Q. Xu, Y. Hu and C. Li, Rapid low-temperature synthesis of hollow $CuS_{0.55}$ nanoparticles for efficient electrocatalytic water oxidation, *Chem. Eng. Sci.*, 2019, **195**, 665-670.

9 Z. Wu, Z. Zou, J. Huang and F. Gao, $NiFe_2O_4$ Nanoparticles/NiFe Layered Double-Hydroxide Nanosheet Heterostructure Array for Efficient Overall Water Splitting at Large Current Densities, *ACS Appl. Mater. Interfaces*, 2018, **10**, 26283-26292.

10 P. W. Menezes, C. Panda, S. Garai, C. Walter, A. Guiet and M. Driess, Structurally Ordered Intermetallic Cobalt Stannide Nanocrystals for High-Performance Electrocatalytic Overall Water-Splitting, *Angew. Chem. Int. Ed.*, 2018, **57**, 15237-15242.

11 Y. K. Kim, J. H. Kim, Y. H. Jo and J. S. Lee, Precipitating Metal Nitrate Deposition of Amorphous Metal Oxyhydroxide Electrodes Containing Ni, Fe, and Co for Electrocatalytic Water Oxidation, *ACS Catal.*, 2019, **9**, 9650-9662.

12 X. Lu and C. Zhao, Electrodeposition of hierarchically structured three-dimensional nickel-iron electrodes for efficient oxygen evolution at high current densities, *Nat. Commun.*, 2015, **6**, 6616.

13 Z. Wu, Z. Zou, J. Huang and F. Gao, Fe-doped NiO mesoporous nanosheets array for highly efficient overall water splitting, *J. Catal.*, 2018, **358**, 243-252.

14 Q. Zhang, D. Yan, Z. Nie, X. Qiu, S. Wang, J. Yuan, D. Su, G. Wang and Z. Wu, Iron-Doped NiCoP Porous Nanosheet Arrays as a Highly Efficient Electrocatalyst for Oxygen Evolution Reaction, *ACS Appl. Energy Mater.*, 2018, **1**, 571-579.

15 W. Zhu, X. Yue, W. Zhang, S. Yu, Y. Zhang, J. Wang and J. Wang, Nickel sulfide microsphere film on Ni foam as an efficient bifunctional electrocatalyst for overall water splitting, *Chem. Commun.*, 2016, **52**, 1486-1489.

16 M. A. R. Anjum, M. S. Okyay, M. Kim, M. H. Lee, N. Park and J. S. Lee, Bifunctional sulfur-doped cobalt phosphide electrocatalyst outperforms all-noble-metal electrocatalysts in alkaline electrolyzer for overall water splitting, *Nano Energy*, 2018, **53**, 286-295.

17 Y. Xu, L. Xie, D. Li, R. Yang, D. Jiang and M. Chen, Engineering $Ni(OH)_2$ Nanosheet on $CoMoO_4$ Nanoplate Array as Efficient Electrocatalyst for Oxygen Evolution Reaction, *ACS Sustainable Chem. Eng.*, 2018, **6**, 16086-16095.